



Mechanical Engineering

Numerical investigation of inward solidification inside spherical capsule by using temperature transforming method

Mustafa Asker ^a , Hadi Ganjehsarabi ^b, M. Turhan Coban ^c Show more<https://doi.org/10.1016/j.asej.2016.02.009>[Get rights and content](#)Under a Creative Commons [license](#)[open access](#)

Abstract

In this study, a numerical analysis of the inward [solidification](#) of [phase change material](#) inside spherical capsule is carried out. The spherical capsule that is subjected to convection from the outside surface initially is not at its melting temperature. The control volume approach and temperature transforming method are applied to solve the [dimensionless](#) energy equation. The model solution results are validated through a comparison with published experimental data for similar case and it shows a considerably good agreement. The analysis results show that the larger diameter spherical capsules have significantly greater [solidification time](#) compared to those with smaller diameters of spherical capsules. In addition, the [entropy generation](#) inside spherical capsule is analyzed. It is found that the entropy generation increases with increasing sphere capsule diameter, attains a maximum and then decreases.



Previous

Next



Keywords

Entropy generation; Phase change material; Solidification; Spherical capsules

Nomenclature

 Bi [Biot number](#), $Bi = \frac{hr_0}{k_i}$ c

specific heat, J/kg K

 C [dimensionless](#) specific heat, $C = \frac{(\rho c)}{\rho_L c_L}$ C_{sl} [dimensionless](#) specific heat, $C_{SL} = \frac{(\rho_s c_L)}{\rho_L c_L}$

D

diameter of the spherical capsule, m

 Fo Fourier number, $Fo = \frac{\alpha_L t}{r_o^2}$ g gravitational acceleration, m/s^2 h convective heat transfer coefficient, $W/m^2 K$ H

enthalpy

 k thermal conductivity, $W/m K$ K dimensionless thermal conductivity, $K = \frac{k}{k_L}$ L latent heat of fusion, J/kg Nu Nusselt number, $Nu = \frac{\bar{h} D}{k_{cf}}$ Pr

Prandtl number

 r

radial position, m

 r_o

radius of the spherical capsule, m

 R dimensionless radial position, $R = \frac{r}{r_o}$ Ra Rayleigh number, $Ra_D = \frac{g\beta(T_s - T_{cf})D^3}{\alpha\nu}$ S source term, $S = \frac{s^*}{\rho_L c_L (T_m - T_{cf})}$ \dot{S}_{gen}''' entropy generation per unit volume, $W/m^3 K$ Ste Stefan number, $Ste = \frac{c_L (T_m - T_{cf})}{L}$ T

temperature, K

 T_i

initial temperature, K

 T_m

phase change temperature, K

T_s
surface temperature of the spherical container, K

T_{cf}
coolant fluid temperature, K

Greek symbols

α
thermal diffusivity, m^2/s

β
coefficient of thermal expansion, $1/\text{K}$

Δr
radial distance between grid points, m

ΔR
dimensionless radial distance between grid points

Δt
time step, s

μ
dynamic viscosity, kg/ms

θ
dimensionless temperature, $\theta = \frac{T - T_m}{T_m - T_{cf}}$

$\delta\theta_m$
dimensionless phase-change temperature range

ρ
density, kg/m^3

Subscripts

cf
coolant fluid

e
control volume face between P and E

E
neighbor grid point on the east side

k
time level

L
liquid phase

P
central grid point

s
solid phase, Interface

w
control volume face between P and W

W

neighbor grid point on the west side

 wf

working fluid

Superscript

0

previous time step

1. Introduction

During the last decade, [thermal energy storage](#) (TES) systems and applications have developed and been extended to industrial use in many countries.

Latent heat [thermal energy storage system](#) is considered as one of the suitable methods of storing thermal energy because of their advantages in providing high storage density and has the capacity to store energy with small temperature difference [1]. [Phase change material](#) (PCM) encapsulation can be enhanced in various ways using cylindrical geometries or spherical capsules. The spherical capsules offer advantages over cylindrical capsules, including high [energy storage capacity](#) per unit of volume and easy packing into the storage tank.

Several detailed reviews of the phase-change materials and their various applications in thermal energy storage systems have been published by many researchers [2], [3], [4], [5], [6].

The investigation of the [thermal behavior](#) of PCMs in spherical capsules plays a key role in designing [latent heat storage](#) systems [7]. Ismail and Moraes [8] investigated numerically and experimentally the effects of varying certain operating parameters on the time for complete [solidification](#) of the various phase-change materials encapsulated in spherical and [cylindrical shells](#). Ismail and Henriquez [9] developed a simplified transient one-dimensional model to simulate a storage system consisted of spherical capsules filled with PCM placed inside a [cylindrical tank](#) fitted with a working fluid circulation system to charge and discharge the storage tank.

Adine and Qarnia [10] presented a numerical study of a latent heat storage unit consisting of a shell-and-tube. The shell space is filled with two phase change materials (PCMs), P116 and n-octadecane, with different melting temperatures. They also investigated the effects of various design parameters such as [heat transfer fluid inlet temperature](#), [mass flow rate](#) and lengths of the PCMs sections on the thermal performances of the latent heat storage unit.

Lamberg and Siren [11] developed a simplified analytical model which predicts the solid–liquid interface location and temperature distribution of the fin in the [solidification process](#) with a constant end-wall temperature in the finned two dimensional PCM storage.

Tao [12] conducted a numerical method for solidification of a saturated liquid in cylinders and spheres. He assumed that the [thermal conductivity](#), heat capacity of solid phase and [convective heat transfer coefficient](#) are constant.

Yang and Zhao [13] developed a feasible technique that combines the numerical calculation and the transformation of [dimensionless variables](#) in [heat diffusion equations](#) in order to analyze the solidification of PCM within a single encapsulated particle. Their results show that the smaller microcapsule can realize the rapid solidification under the constant temperature boundary condition. Pedroso and Domoto [14] studied the total [solidification time](#) in spherical coordinate by using [perturbation method](#). They assumed that thermophysical properties of phase change material and the surface of the sphere are constant.

Riley et al. [15] studied analytically the inward solidification of a sphere and a circular cylinder for which is initially at melting temperature. They assumed that the thermal properties are constant. Their analysis was made for small Stefan number.

Hill and Kucera [16] presented a semi analytical procedure for the problem of freezing a saturated liquid inside spherical container by taking into consideration the effect of radiation at the container surface.

Prud'homme et al. [17] applied strained coordinate method to analyze the inward solidification of slabs, cylinders and spheres for three different types of boundary conditions. They assumed constant thermal properties for the liquid which is initially at the fusion temperature.

Ismail and Henriquez [18] presented numerical solution based upon finite difference approximations for the solidification of phase change material in a spherical container under constant external wall temperature or convection boundary condition. They carried out a [parametric study](#) of the effects of the diameter of sphere, wall thickness, wall material, external temperature and the initial phase change material temperature on the solidified mass fraction and the time for the complete solidification. In another work, Ismail et al. [19] studied numerically the process of solidification of water inside spherical capsule. They solved their model by using [finite difference approach](#) and moving grid scheme and compared their results with an earlier experimental work results. Furthermore, they performed a parametric study of the effects of the material of the shell, initial temperature of the phase change material and the external temperature of the spherical capsule on the solidified mass fraction and the time for the complete solidification.

Eames and Adref [20] investigated experimentally freezing and melting processes for water contained in spherical elements of the type used in thermal (ice) storage systems. Bilir and Ilken [21] reported the result of a numerical study on the inward solidification of a liquid phase change material encapsulated in cylindrical and spherical container with a third kind of boundary condition. They used [enthalpy method](#) with control volume approach. They derived correlations that express the [dimensionless](#) total solidification time of the PCM in terms of Stefan Number, [Biot Number](#) and Superheat Parameter.

Chan and Tan [22] studied the solidification of n-hexadecane inside a spherical enclosure. They showed that the solidification phase front propagates uniformly inward toward the center of the sphere.

Veerappan et al. [23] developed an analytical model based on quasi steady approximations for solidification and melting of PCMs in a spherical container where the sphere is initially at its melting temperature. The external surface of the spherical shell is assumed to be at [isothermal](#) boundary conditions. However, the resistance of the outer shell is neglected. They investigated the effect of design parameters such as size of the spherical capsule, external fluid temperature and the initial PCM temperature on the solidified mass fraction and the time for complete solidification.

In order to solve phase change problems, various numerical methods such as the enthalpy method [24], [25], the equivalent heat capacity method [26] and the temperature-transforming model [27] have been developed. The temperature-transforming model eliminates the time-step and grid-size restrictions. It is also insensitive to the [phase-change temperature](#) range [28]. The temperature transforming model has been used to solve many different problems related to latent heat thermal energy storage systems [29], [30], [31].

The primary objective of this work was to analyze the inward solidification inside spherical capsule which is initially not at its melting temperature under the effect of convection at the outside surface. The specific objectives are as follows:

- To investigate the solidification of phase change material inside spherical capsule.
- To solve the problem numerically by using control volume approach and temperature transforming method.
- To examine the effect of sphere diameter and coolant fluid temperature on the time elapsed for a total solidification.
- To determine the effect of various design parameters such as sphere diameter and coolant fluid temperature on entropy generation.

2. Mathematical model

The present analysis will consider one spherical capsule with radius r_o . The spherical capsule is filled with [phase change material](#) initially at T_i , which is higher than its melting temperature T_m . Water is used as a phase change material. The thermophysical properties of water are given in [Table 1](#). The outside surface of the spherical capsule is subjected to [convection heat transfer](#). The coolant temperature is kept at T_{cf} . The following assumptions are made:

- The thermophysical properties of PCM are independent of temperature but they differ for the solid and liquid phases of the PCM.
- The PCM is homogenous and isotropic.
- The effect of [natural convection](#) inside the PCM liquid is neglected.

Table 1. Thermophysical properties of water.

Properties	Water (liquid)	Water (solid)
Density, kg/m ³	999.8	916.8
Specific heat, kJ/kg K	4210	2040
Thermal conductivity, W/m K	0.567	1.88
Melting temperature, °C	0	
Latent heat of fusion, kJ/kg	333,500	

It should be noted that the subcooling phenomenon, encountered especially in water crystallization, is neglected in the proposed model. In addition, the volume expansion due to [solidification](#) of water is also ignored. The [heat conduction](#) in the PCM is formulated by a temperature transforming method using a [fixed grid](#) numerical model [27]. This model assumes that [solidification process](#) occurs over a range of [phase change temperatures](#) from $(T_m - \delta T_m)$ to $(T_m + \delta T_m)$, but it can also be used to simulate the solidification process occurring at a single temperature by taking a small range of phase change temperature, $2\delta T_m$. This method has the advantage of eliminating the time step and grid size limitations that are normally encountered in other fixed grid methods [29].

Based upon the aforementioned assumptions, the governing energy equation in spherical coordinate can be written as follows:

$$\frac{\partial H}{\partial t} = \frac{1}{r^2} \frac{\partial}{\partial r} \left(kr^2 \frac{\partial T}{\partial r} \right) \quad (1)$$

The relation between the enthalpy and temperature can be expressed in linear form as follows:

$$H = cT + s^* \quad (2)$$

where c , s^* are the dimensional specific heat and source term, respectively. Eq. (1) can be nondimensionalized by using the following [dimensionless parameters](#):

$$R = \frac{r}{r_0}, \quad C = \frac{\rho c}{\rho_L c_L}, \quad \theta = \frac{T - T_m}{T_m - T_{cf}}, \quad \delta\theta_m = \frac{\delta T}{T_m - T_{cf}}, \quad K = \frac{k}{k_L}, \quad Fo = \frac{\alpha_L t}{r_0^2} \\ Bi = \frac{hr_0}{k_L}, \quad S = \frac{s^*}{\rho_L c_L (T_m - T_{cf})}, \quad Ste = \frac{c_L (T_m - T_{cf})}{L} \quad (3)$$

Here s^* is the dimensional source term. By using the aforesaid [dimensionless](#) parameters, the [dimensionless forms](#) of energy equation for spherical capsule can be written as follows:

$$\frac{\partial(C\theta)}{\partial Fo} = \frac{1}{R^2} \frac{\partial}{\partial R} \left[KR^2 \frac{\partial \theta}{\partial R} \right] - \frac{\partial S}{\partial Fo} \quad (4)$$

where

$$C(\theta) = \begin{cases} C_{sl} & \theta < -\delta\theta_m & \text{Solid} \\ \frac{1}{2}(1 + C_{sl}) + \frac{1}{2 Ste \delta\theta_m} & -\delta\theta_m \leq \theta \leq \delta\theta_m & \text{Mushy} \\ 1 & \theta > \delta\theta_m & \text{Liquid} \end{cases} \quad (5)$$

$$S(\theta) = \begin{cases} C_{sl}\delta\theta_m & \theta < -\delta\theta_m & \text{Solid} \\ \left[\frac{1}{2}\delta\theta_m(1 + C_{sl}) + \frac{1}{2\delta\theta_m} \right] & -\delta\theta_m \leq \theta \leq \delta\theta_m & \text{Mushy} \\ C_{sl}\delta\theta_m + \frac{1}{\delta\theta_m} & \theta > \delta\theta_m & \text{Liquid} \end{cases} \quad (6)$$

$$K(\theta) = \begin{cases} K_{sl} & \theta < -\delta\theta_m & \text{Solid} \\ K_{sl} + \frac{(1-K_{sl})(\theta+\delta\theta_m)}{2\delta\theta_m} & -\delta\theta_m \leq \theta \leq \delta\theta_m & \text{Mushy} \\ 1 & \theta > \delta\theta_m & \text{Liquid} \end{cases} \quad (7)$$

A mushy region is formed where solid coexists with liquid in equilibrium. According to temperature transforming method, mushy phase will occur when the temperature at node (i) satisfies the condition of $-\delta\theta_m \leq \theta \leq \delta\theta_m$. The values of $C(\theta)$, $S(\theta)$ and $K(\theta)$ at the mushy phase can be calculated by using Eqs. (5), (6), (7), respectively.

The initial condition for Eq. (4) is

$$Fo = 0 \rightarrow \theta = \theta_i \quad (8)$$

While the boundary conditions for Eq. (4) are

$$R = 0 \rightarrow \frac{\partial\theta}{\partial R} = 0 \quad (9)$$

$$R = 1 \rightarrow K \frac{\partial\theta}{\partial R} = -Bi(\theta + 1) \quad (10)$$

In the current study the model of Ismail et al. [19] is used in which the spherical capsule is immersed in a pool of ethanol. The thermophysical properties of ethanol are obtained from Reid et al. [32]. The convection heat transfer coefficient can be calculated by using Churchill correlations as follows [33]:

$$\overline{Nu_D} = \frac{hD}{k_{ef}} = 2 + \frac{0.589Ra_D^{1/4}}{[1 + (0.469/P_r)^{9/16}]^{4/9}} \quad (11)$$

Here Rayleigh number can be calculated as follows:

$$Ra_D = \frac{g\beta(T_s - T_{ef})D^3}{\alpha\nu} \quad (12)$$

2.1. Solution method

The problem is solved by using the control volume approach described by Versteeg and Malalasekera [34], and the dimensionless energy Eq. (4) is integrated over the control volume and time as follows:

$$\int_V \int_{Fo} \frac{\partial(C\theta)}{\partial Fo} dV dFo = \int_V \int_{Fo} \frac{1}{R^2} \frac{\partial}{\partial R} \left[KR^2 \frac{\partial\theta}{\partial R} \right] dV dFo - \int_V \int_{Fo} \frac{\partial S}{\partial Fo} dV dFo \quad (13)$$

The dimensionless energy Eq. (4) is integrated across the control volume in r direction and time. Performing the integration and rearranging it, the following finite volume equations can be obtained as follows:

$$\frac{C_P\theta_P - C_P^0\theta_P^0}{\Delta Fo} \frac{(R_e^3 - R_w^3)}{3} = \left[K_e R_e^2 \frac{\theta_E - \theta_P}{\Delta R_e} - K_w R_w^2 \frac{\theta_P - \theta_W}{\Delta R_w} \right] - \frac{S_P - S_P^0}{\Delta Fo} \frac{(R_e^3 - R_w^3)}{3} \quad (14)$$

where θ_P^0 is the dimensionless temperature at the previous time step. C_P^0 and S_P^0 are the dimensionless specific heat and source term at previous time step, respectively. R_e and R_w are the dimensionless radii for the control volume interfaces at e and w , respectively. K_e and K_w are thermal conductivities for the control volume interfaces at e and w , respectively.

The dimensionless thermal conductivity at the control surface is calculated by using harmonic mean which is described by Patankar [35]. Fig. 1 illustrates the discretization of the control volume for nodal points. The discretized equation can be written as follows:

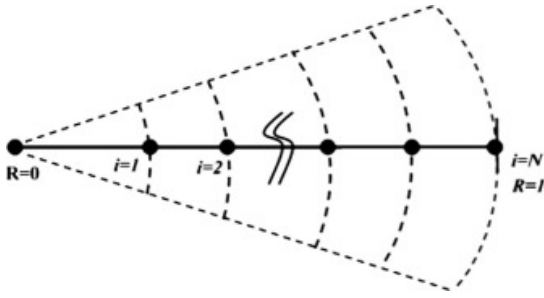
$$a_P\theta_P = a_E\theta_E + a_W\theta_W + b \quad (15)$$

where

$$a_E = \frac{K_e R_e^2}{\Delta R_e}, \quad a_W = \frac{K_w R_w^2}{\Delta R_w} \quad (16)$$

$$b = \left[\frac{C_P \theta_P^0}{\Delta Fo} - \frac{S_P - S_P^0}{\Delta Fo} \right] \frac{(R_e^3 - R_w^3)}{3} \quad (17)$$

$$a_P = a_E + a_W + \frac{C_P \theta_P}{\Delta Fo} \frac{(R_e^3 - R_w^3)}{3} \quad (18)$$



Download : [Download high-res image \(35KB\)](#)

Download : [Download full-size image](#)

Figure 1. Nodal point for the control volume.

The algebraic equations have been solved by using Thomas algorithm. Since the dimensionless energy equation is nonlinear heat conduction equation, iteration is needed at each time step which is declared as follows:

$$|\theta_i^{k+1} - \theta_i^k| \leq 10^{-9} \quad (19)$$

During the calculation process, the energy balance is checked to verify the numerical results, and thus at each time step, the change in the stored energy of the PCM must be equal to the total heat rejected from the sphere as follows:

$$\int_0^{Fo} 4\pi R_P^2 Bi(\theta_P + 1) dFo = \sum_{i=1}^N \int_{R_w}^{R_e} 4\pi(H^* - H_0^*) R^2 dR \quad (20)$$

where N represents the number of nodes.

The left-hand side of Eq. (20) represents the heat rejected from the PCM while the right hand-side represents the energy stored in the PCM. The numerical deviation between two sides of Eq. (20) is taken less than 0.00000001%.

3. Entropy generation

After the temperature distribution is obtained it's possible to calculate the local entropy generation. The entropy generation rate per unit volume may be expressed based on the second law of thermodynamics in the following manner [36]:

$$\dot{S}_{gen}'' = \frac{q + \left(\frac{\partial q}{\partial r}\right) dr}{T + \left(\frac{\partial T}{\partial r}\right) dr} - \frac{q}{T} + \rho \frac{\partial s}{\partial t} dr \quad (21)$$

The first two terms in the right side of Eq. (21) represent the entropy transfer associated with heat transfer, and the last term represents the rate of entropy accumulation in the element. Dividing Eq. (21) by dr , the local entropy generation becomes the following:

$$\dot{S}_{gen}''' = \frac{1}{T} \frac{\partial q}{\partial r} - \frac{q}{T^2} \frac{\partial T}{\partial r} + \rho \frac{\partial s}{\partial t} \quad (22)$$

if $\partial s = \partial u / T$, where u is internal energy, inside the element dr

$$\rho \frac{\partial s}{\partial t} = \frac{\rho}{T} \frac{\partial u}{\partial t} \quad (23)$$

From the first law of thermodynamics, written for one point in the convective medium, $(\delta u / \delta t) = -\delta q / \delta x$, so we can write down Eq. (21) as

$$\rho \frac{\partial s}{\partial t} = -\frac{1}{T} \frac{\partial q}{\partial r} \quad (24)$$

Combining Eq. (21) with Eq. (22) we obtain entropy generation as

$$\dot{S}_{gen}''' = -\frac{q}{T^2} \frac{\partial T}{\partial r} \quad (25)$$

Applying Fourier's law, the local entropy generation rate per unit volume for one dimensional spherical coordinate becomes [36]:

$$\dot{S}_{gen}''' = \frac{k}{T^2} \left(\frac{\partial T}{\partial r} \right)^2 \quad (26)$$

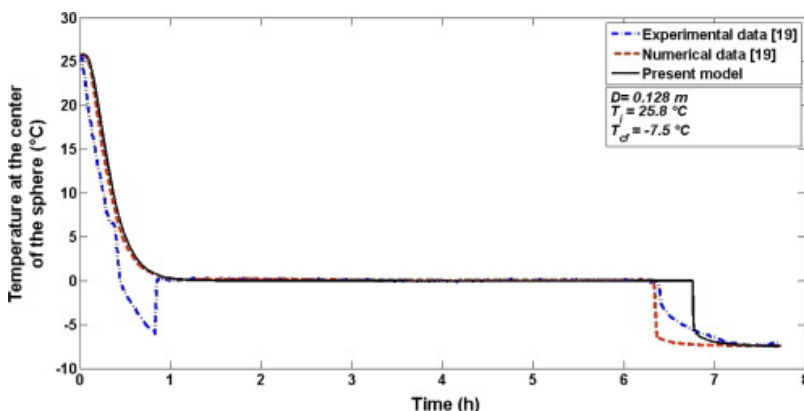
Since the viscous effect is neglected then the total entropy generation per unit volume can be determined by integrating Eq. (26) over the volume. It should be noted here that Eq. (26) is derived by applying the second law of thermodynamics on small element. In addition, the element size is small enough so that the thermodynamic state of the fluid inside the element is considered independent of position. However, the thermodynamic state of the element may be changed with time [36].

4. Results and discussion

A numerical investigation has been performed to study the effects of design parameters on solidification and entropy generation of phase change material inside a spherical capsule. The finite volume method is used in order to solve the governing equations.

In this study, the solidification process starts from the outside surface which is in contact with the coolant fluid, and proceeds inward toward the center of the sphere due to the heat transfer mechanism. The analysis presented here is the case of pure conduction and convection effect in the liquid phase is neglected. It's because of the fact that the initial temperature of the spherical capsule is considered to be near the phase change temperature, and as a result, the natural convection effect inside the liquid phase can be neglected. The solidification process is completed when all the liquid is solidified and the system has reached its thermal equilibrium with outside coolant temperature. Throughout the solution, the number of grids is selected to be $N = 500$, the time step is $\Delta t = 0.1$ and the phase change temperature range is 0.01.

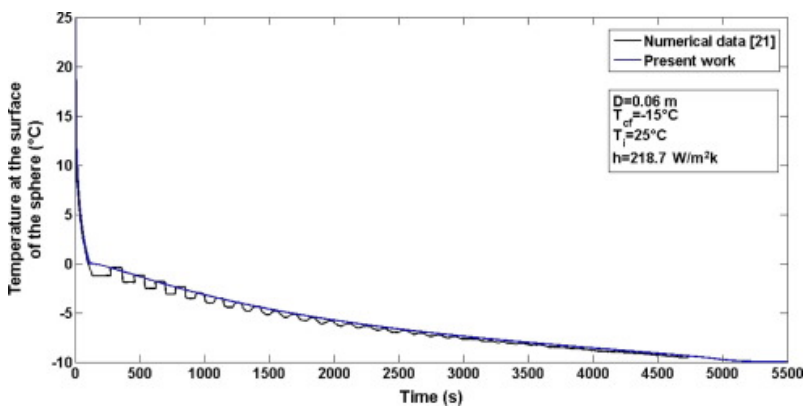
In order to verify and validate the numerical model used in this work, the result are compared with the existing published numerical and experimental data obtained by [19]. The present numerical results for temperature variation of phase change material at the center of sphere and the numerical and experimental data from [19] are depicted in Fig. 2. In this figure, the initial temperature, the coolant fluid temperature and the diameter of spherical capsule are taken as 25.8 °C, -7.5 °C and 0.128 m, respectively. Fig. 2 shows a good agreement between the present numerical model results and the published experimental data which gives more confidence in the method of tackling this problem. Bilir and İlken [21] presented figure for the surface temperature of a sphere with time which can be verified against that solution. The numerical model was implemented at fixed values of $D = 0.06$ m, $T_{cf} = -15$ °C, $T_i = 25$ °C, and $h = 218.7$ W/m² K and the results are illustrated in Fig. 3. Excellent agreement between the obtained result and published data is verified. In addition, no oscillations in the surface temperature are occurred and this result also shows the accuracy of the numerical model.



Download : [Download high-res image \(154KB\)](#)

Download : [Download full-size image](#)

Figure 2. Comparison of present model results with the experimental and numerical data taken from [19].



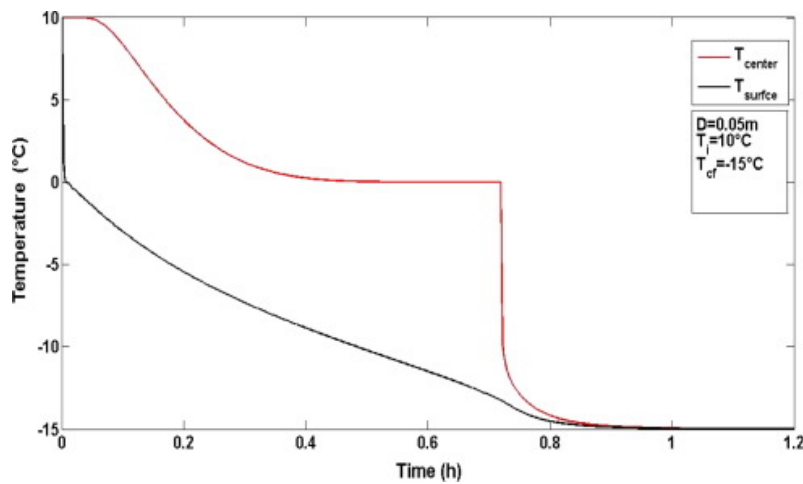
Download : [Download high-res image \(141KB\)](#)

Download : [Download full-size image](#)

Figure 3. Comparison of the surface temperature of a sphere with Ref. [21].

In order to examine the stability of temperature transforming method, the changes in interface position and the temperature at the center of spherical capsule as time is varied are calculated for several phase change temperature range values $\delta T = 0.001$, $\delta T = 0.01$, $\delta T = 0.05$ and $\delta T = 0.1$. It is found that the method is insensitive to the phase change temperature range. As a result, a small phase change temperature range is used to simulate the [solidification front](#).

The variation of surface temperature (T_s) and temperature at the center of the spherical capsule (T_{center}) is illustrated in [Fig. 4](#). This figure shows that the central part of the capsule keeps existing in its liquid phase for approximately 0.4 h while the solid phase at the center starts initiating in approximately 0.72 h. The mushy phase occurs between these two periods. The reason of sudden decrease in the temperature at the center of the spherical capsule at approximately 0.72 h is due to removing sensible heat from the solidified mass while phase change is occurred at the transformation from mushy phase to solid phase. After approximately 1.1 h the system reaches its thermal equilibrium and the solidification process is completed. In [Fig. 4](#), the [dimensionless](#) phase change temperature at the beginning of solidification would be $\delta\theta_m = 6.666 \times 10^{-4}$. The outer surface of the phase change material is at liquid phase which is the case of $\theta > 6.667 \times 10^{-4}$, and the value of dimensionless specific heat, [thermal conductivity](#) and source term at that point would be $C = 1$, $K = 1$ and $S = 5.2814$, respectively. The temperature distribution is calculated from Eq. (14). The temperature continuously decreases while the value of C , K and S is kept constant at liquid region. The mushy phase is occurred at the node in the range of $-6.667 \times 10^{-4} \leq \theta \leq 6.667 \times 10^{-4}$. In this case the value of dimensionless specific heat and source term at that point will be changed as $C = 3961.53$ and $S = 2.641$, respectively. However, the thermal conductivity varies linearly with temperature. In the range of $\theta < -6.667 \times 10^{-4}$, the liquid phase is occurred and in this case $C = 0.4443$, $K = 3.3156$ and $S = 2.962 \times 10^{-4}$, respectively. The process continues until the center of the sphere is solidified completely and the temperature of the center of sphere is equal to coolant fluid temperature.

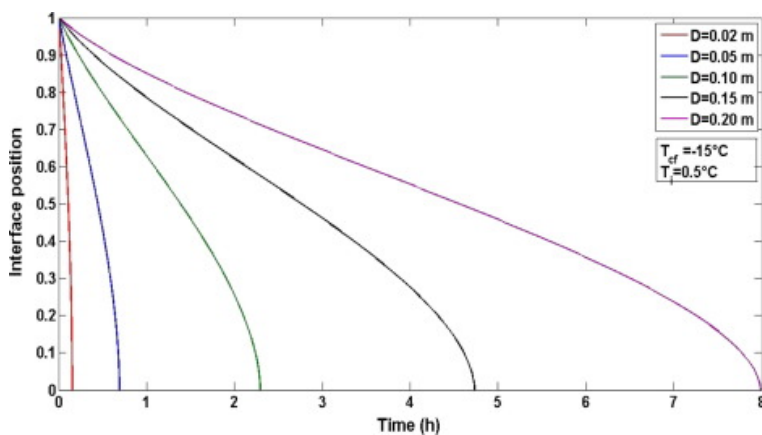


[Download : Download high-res image \(119KB\)](#)

[Download : Download full-size image](#)

Figure 4. Transient distributions of surface temperature and center temperature of sphere capsule.

Fig. 5 shows the transient variation of the solid–liquid interface position for different sphere diameters $D = 0.02$ m, $D = 0.05$ m, $D = 0.1$ m, $D = 0.15$ m and $D = 0.2$ m. The initial temperature is 0.5°C and the coolant fluid temperature is -15°C . It can be seen that at $D = 0.02$ m the time elapsed for complete solidification of the liquid is found to be 0.166 h (10 min) while its 8.6 h at $D = 0.2$ m. It can also be observed that larger diameters of spherical capsule have significantly greater solidification time compared to those of smaller diameters of spherical capsules. Since the ice forms the first layer at the last grid node (N) and as the ice thickness increases toward the center of the sphere the thermal resistance will also increase; therefore, the distance of heat transfer to take place will be larger as the sphere diameter varies increasing from $D = 0.02$ m to $D = 0.2$ m.



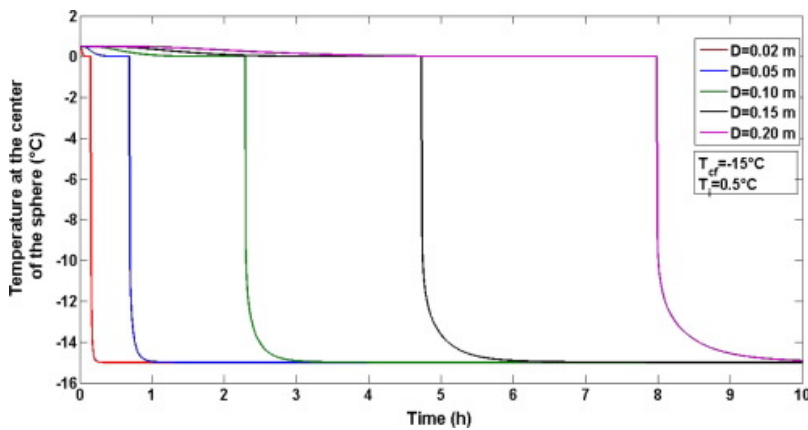
[Download : Download high-res image \(150KB\)](#)

[Download : Download full-size image](#)

Figure 5. Effects of the diameter of sphere capsule on interface position.

For the same sphere diameters and temperature conditions Fig. 6 shows the behavior of temperature profile at the center of the sphere with respect to time as the diameter of the sphere capsule increases from 0.02 m to 0.2 m. It should be noted that for all the cases considered, fixed values of $T_i = 0.5^\circ\text{C}$ and $T_{cf} = -15^\circ\text{C}$ with variable sphere capsule diameters $D = 0.02$ – 0.2 m are used. The temperature at the center of spherical capsule at liquid state decreases until it eventually becomes constant as it passes to the mushy phase, suddenly drops to the solid phase and then further decreases slightly. It can be observed that spherical capsules with smaller diameters require significantly lower

solidification time compared to those with larger diameters because PCMs spheres with smaller diameters have higher solidification rates.

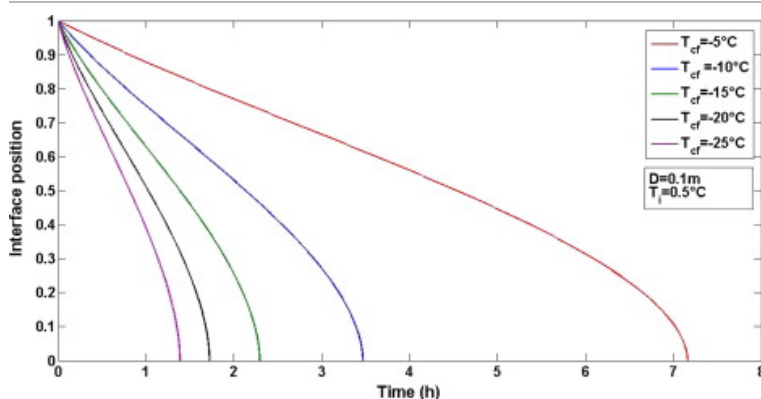


[Download](#) : [Download high-res image \(145KB\)](#)

[Download](#) : [Download full-size image](#)

Figure 6. Variation of the temperature at the center of the sphere with respect to the time and the diameter of spherical capsule.

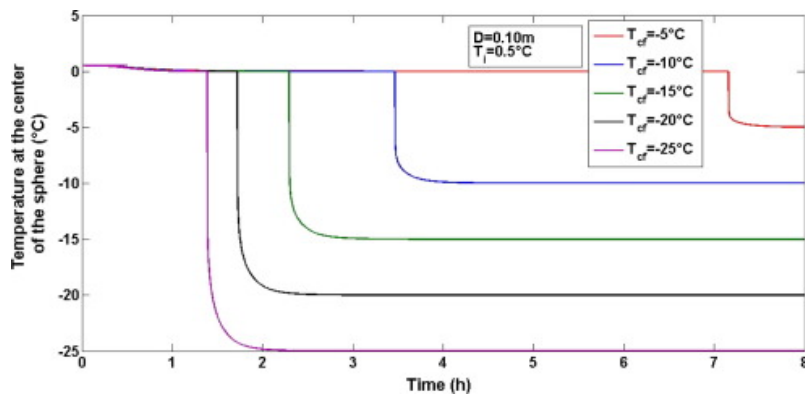
The effect of the coolant fluid temperature on the interface position is depicted in Fig. 7. The coolant fluid temperature is varied from -5°C to -25°C in steps of 5°C , while initial temperature and the diameter of spherical capsules are taken as 0.5°C and 0.1 m , respectively. At $T_{cf} = -5^{\circ}\text{C}$ the time for total solidification is 7.6 h while at $T_{cf} = -25^{\circ}\text{C}$ the time for complete solidification is 1.5 h . It can be seen in this figure that reducing coolant fluid temperature from -5°C to -25°C significantly decreases the time for complete phase change due to the higher convective heat transfer rate. The temperature variation of phase change material at the center of spherical capsule at different coolant fluid temperatures is illustrated in Fig. 8. As shown in Fig. 8, for a given value of the time, the temperature at the center of sphere capsule decreases and eventually becomes constant, drops suddenly and then finally decreases slightly before it becomes stabilized. It is concluded that the lower is the coolant fluid temperature, the shorter is the solidification time in sphere capsule. Fig. 9 presents the effect of the initial temperature on the interface position. The initial temperature was varied from 5°C to 25°C in steps of 5°C , while keeping the other parameters constant. As can be seen from Fig. 9, decreasing initial temperature from 25°C to 5°C has very small effect on the time for complete phase change.



[Download](#) : [Download high-res image \(154KB\)](#)

[Download](#) : [Download full-size image](#)

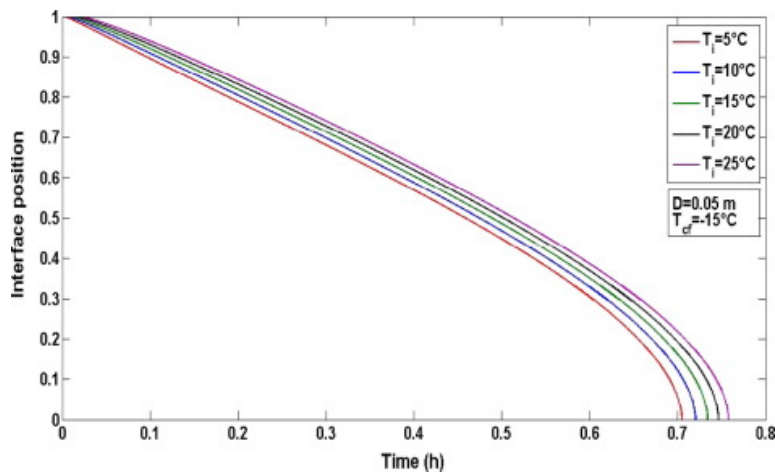
Figure 7. Variation of interface position with respect to the solidification time and the coolant fluid temperature.



Download : [Download high-res image \(136KB\)](#)

Download : [Download full-size image](#)

Figure 8. Variation of the temperature at the center of the sphere with respect to the time and the coolant fluid temperature.

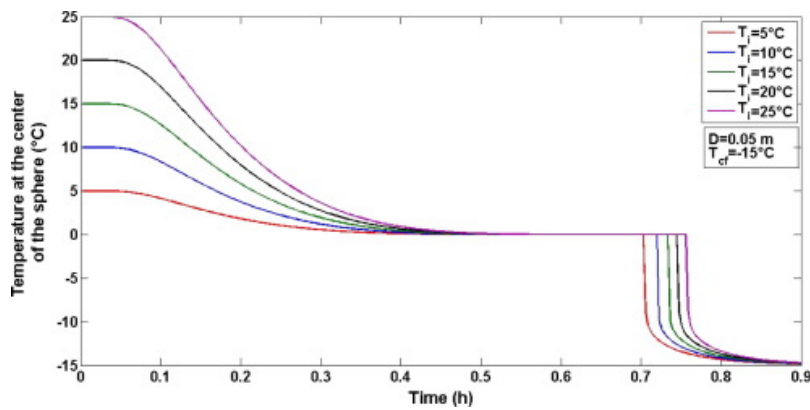


Download : [Download high-res image \(206KB\)](#)

Download : [Download full-size image](#)

Figure 9. Variation of interface position with respect to the solidification time and the initial temperature.

Fig. 10 illustrates the temperature distribution at the center of the sphere capsule for various values of initial temperatures T_i , ($T_i = 5, 10, 15, 20, 25$ °C). In this figure, the coolant fluid temperature and the diameter of spherical capsule are fixed and taken as -15 °C and 0.05 m, respectively. Beside, the diameter of spherical capsule is considered to be in small value in order to satisfy the assumption of ignoring natural convection effect inside the liquid phase. For particular value of the initial temperature, the magnitude of temperature is higher for higher value of the initial temperature. For a given value of the time, at $T_i = 10$ °C, the temperature at the center of sphere capsule is constant for values of the time between 0.0 and 0.08 h (4.8 min) and then decreases and eventually becomes constant as it passes to mushy phase for values of the time between 0.4 h (24 min) and 0.72 h (43.2 min), drops suddenly and then finally decreases slightly to reach the value of -15 °C at values of the time greater than 0.9 h (54 min).

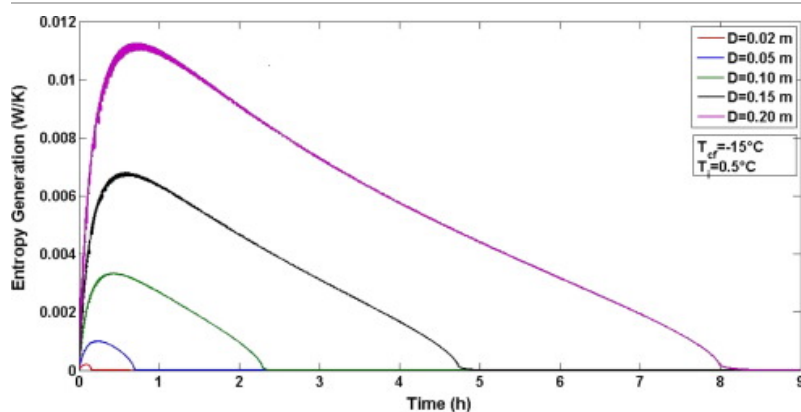


Download : [Download high-res image \(170KB\)](#)

Download : [Download full-size image](#)

Figure 10. Variation of the temperature at the center of the sphere with respect to the time and the initial temperature.

Fig. 11 shows the variation of entropy generation with respect to solidification time for different values of sphere diameter. In this figure, the diameter of the spherical capsule has significant effect on the entropy generation. It can be observed that an increase in the diameter of spherical capsule results in an increase in entropy generation. For particular value of the time, the entropy generation is higher for higher value of the diameter of spherical capsule.

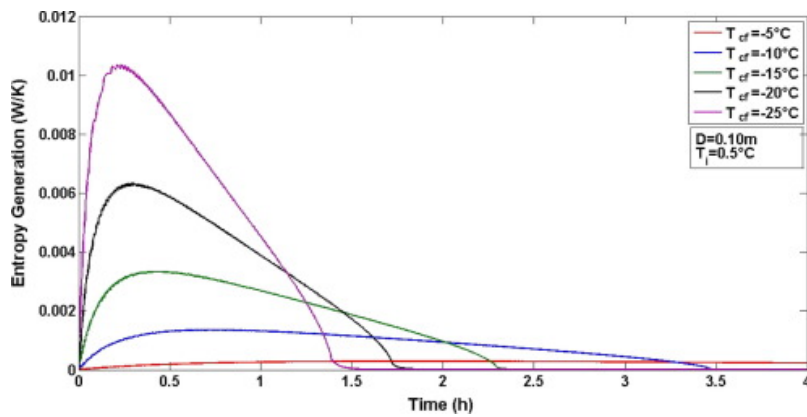


Download : [Download high-res image \(155KB\)](#)

Download : [Download full-size image](#)

Figure 11. Effect of the diameter of sphere capsule on entropy generation.

According to Eq. (25), entropy generation is directly proportional to heat transfer rate and temperature gradient. At the beginning of the solidification process, the heat transfer rate increases rapidly until it reaches to interphase position. Therefore, the entropy generation increases sharply at the beginning up to a maximum point. After the peak point, the solidification rate and heat transfer rate decrease smoothly because of the increasing thermal resistance. As a result, the entropy generation drops off to its lowest value where the solidification time is completed. The effect of the coolant fluid temperature on the entropy generation is depicted in Fig. 12. In this figure, initial temperature and the diameter of spherical capsule are taken as 0.5 °C and 0.1 m, respectively. For particular value of the time, the magnitude of entropy generation is higher for lower value of the coolant fluid temperature. For a given value of the coolant fluid temperature, the entropy generation increases with solidification time, attains a maximum and then decreases.



Download : [Download high-res image \(161KB\)](#)

Download : [Download full-size image](#)

Figure 12. Effect of the coolant fluid temperature on [entropy generation](#).

5. Conclusions

The inward [solidification](#) of a [phase change material](#) inside spherical capsule is analyzed numerically by using temperature transforming method. Furthermore, a parametric study is conducted to evaluate the effect of the varying selected design parameters such as sphere diameter and coolant fluid temperature on [solidification time](#) and [entropy generation](#). The model is validated with the experimental published data taken from the literature. The temperature at the center and at the surface of the sphere with respect to time is determined over a range of operating conditions. The following specific concluding remarks can be drawn:










- Small diameter of sphere capsules has significantly lower solidification time compared to larger diameters of sphere capsule.
- The diameter of the spherical capsule has a major effect on entropy generation as the entropy generation increases with increasing diameter of the sphere.
- Selecting a lower coolant fluid temperature results in considerable drop in entropy generation.
- In this context, the diameter of sphere capsule and coolant fluid temperature play an important role in the designing and assessing the [thermal energy storage systems](#).

[Recommended articles](#)

[Citing articles \(2\)](#)

References

- [1] A. Sharma, V.V. Tyagi, C.R. Chen, D. Buddhi
Review on thermal energy storage with phase change materials and applications
Renew Sustain Energy Rev, 13 (2) (2009), pp. 318-345
[Article](#) [Download PDF](#) [View Record in Scopus](#) [Google Scholar](#)
- [2] M.M. Farid, A.M. Khudhai, S.A.K. Razack, S.A. Al-Hallaj
Review on phase change energy storage: materials and applications
Energy Convers Manage, 45 (2004), pp. 1597-1615
[Article](#) [Download PDF](#) [View Record in Scopus](#) [Google Scholar](#)
- [3] B. Zalba, J.M. Marin, L.F. Cabeza, H. Mehling
Review on thermal energy storage whit phase change: materials, heat transfer analysis and applications
Appl Therm Eng, 23 (2003), pp. 251-283
[Article](#) [Download PDF](#) [View Record in Scopus](#) [Google Scholar](#)

- [4] A. Abhat
Low temperature latent heat thermal energy storage. Heat storage materials
Sol Energy, 30 (4) (1983), pp. 313-332
[Article](#)  [Download PDF](#) [View Record in Scopus](#) [Google Scholar](#)
- [5] A.F. Regin, S.C. Solanki, J.S. Saini
Heat transfer characteristics of thermal energy storage system using PCM capsules: a review
Renew Sustain Energy Rev, 12 (9) (2008), pp. 2438-2458
[Article](#)  [Download PDF](#) [View Record in Scopus](#) [Google Scholar](#)
- [6] P. Verma, Varun, S.K. Singal
Review of mathematical modeling on latent heat thermal energy storage systems using phase-change material
Renew Sustain Energy Rev, 12 (4) (2008), pp. 999-1031
[Article](#)  [Download PDF](#) [View Record in Scopus](#) [Google Scholar](#)
- [7] Y. Dutil, D.R. Rousse, N. Ben Salah, S. Lassue, L. Zalewski
A review on phase-change materials: mathematical modeling and simulations
Renew Sustain Energy Rev, 15 (2011), pp. 112-130
[Article](#)  [Download PDF](#) [View Record in Scopus](#) [Google Scholar](#)
- [8] K.A.R. Ismail, R.I.R. Moraes
A numerical and experimental investigation of different containers and PCM options for cold storage modular units for domestic applications
Int J Heat Mass Transf, 52 (2009), pp. 4195-4202
[Article](#)  [Download PDF](#) [View Record in Scopus](#) [Google Scholar](#)
- [9] K.A.R. Ismail, J.R. Henriquez
Numerical and experimental study of spherical capsules packed bed latent heat storage system
Appl Therm Eng, 22 (2002), pp. 1705-1716
[Article](#)  [Download PDF](#) [View Record in Scopus](#) [Google Scholar](#)
- [10] H.A. Adine, H.E. Qarnia
Numerical analysis of the thermal behaviour of a shell-and-tube heat storage unit using phase change materials
Appl Mathemat Model, 33 (2009), pp. 2132-2144
[Article](#)  [Download PDF](#) [View Record in Scopus](#) [Google Scholar](#)
- [11] P. Lamberg, K. Siren
Approximate analytical model for solidification in a finite PCM storage with internal fins
Appl Mathemat Model, 27 (2003), pp. 491-513
[Article](#)  [Download PDF](#) [View Record in Scopus](#) [Google Scholar](#)
- [12] L.C. Tao
Generalized numerical solutions of freezing a saturated liquid in cylinders and spheres
AIChE J, 13 (1) (1967), pp. 165-169
[CrossRef](#) [View Record in Scopus](#) [Google Scholar](#)
- [13] J. Yang, C.Y. Zhao
Solidification analysis of a single particle with encapsulated phase change materials
Appl Therm Eng, 51 (2013), pp. 338-346
[Article](#)  [Download PDF](#) [View Record in Scopus](#) [Google Scholar](#)
- [14] R.I. Pedroso, G.A. Domoto
Perturbation solutions for spherical solidification of saturated liquids
J Heat Transfer, 95 (1) (1973), pp. 42-46
[CrossRef](#) [View Record in Scopus](#) [Google Scholar](#)
- [15] D.S. Riley, F.T. Smith, G. Poots

The inward solidification of spheres and circular cylinders

Int J Heat Mass Transf, 17 (1974), pp. 1507-1516

[Article](#)  [Download PDF](#) [View Record in Scopus](#) [Google Scholar](#)

[16] J.M. Hill, A. Kucera

Freezing a saturated liquid inside a sphere

Int J Heat Mass Transfer, 26 (1983), pp. 1631-1637

[Article](#)  [Download PDF](#) [View Record in Scopus](#) [Google Scholar](#)

[17] M. Prud'Homme, T.H. Nguyen, D.L. Nguyen

A heat transfer analysis for solidification of slabs, cylinders and spheres

J Heat Transf, 111 (1989), pp. 699-705

[CrossRef](#) [View Record in Scopus](#) [Google Scholar](#)

[18] K.A.R. Ismail, J.R. Henriquez

Solidification of PCM inside a spherical capsule

Energy Convers Manage, 41 (2000), pp. 173-187

[Article](#)  [Download PDF](#) [View Record in Scopus](#) [Google Scholar](#)

[19] K.A.R. Ismail, J.R. Henriquez, T.M. da Silva

A parametric study on ice formation inside a spherical capsule

Int J Thermal Sci, 42 (2003), pp. 881-887

[Article](#)  [Download PDF](#) [View Record in Scopus](#) [Google Scholar](#)

[20] I.W. Eames, K.T. Adref

Freezing and melting of water in spherical enclosures of the type used in thermal (ice) storage systems

Appl Therm Eng, 22 (2002), pp. 733-745

[Article](#)  [Download PDF](#) [View Record in Scopus](#) [Google Scholar](#)

[21] L. Bilir, Z. Ilken

Total solidification time of a liquid phase change material enclosed in cylindrical/spherical containers

Appl Therm Eng, 25 (2005), pp. 1488-1502

[Article](#)  [Download PDF](#) [View Record in Scopus](#) [Google Scholar](#)

[22] C.W. Chan, F.L. Tan

Solidification inside a sphere – an experimental study

Int Commun Heat Mass Transf, 33 (2006), pp. 335-341

[Article](#)  [Download PDF](#) [View Record in Scopus](#) [Google Scholar](#)

[23] M. Veerappan, S. Kalaiselvam, S. Iniyan, R. Goic

Phase change characteristic study of spherical PCMs in solar energy storage

Sol Energy, 83 (2009), pp. 1245-1252

[Article](#)  [Download PDF](#) [View Record in Scopus](#) [Google Scholar](#)

[24] N. Shamsunder, E.M. Sparrow

Analysis of multidimensional conduction phase change via the enthalpy model

ASME J Heat Transf, 97 (1975), pp. 333-340

[View Record in Scopus](#) [Google Scholar](#)

[25] J. Crank

Free and moving boundary problems

Clarendon Press, Oxford, U.K. (1984)



[Google Scholar](#)

[26] C. Bonacina, G. Comini, A. Fasano, A. Primicerio

Numerical solution of phase change problems

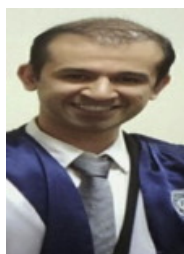
Int J Heat Mass Transf, 16 (1973), pp. 1825-1832

[Article](#)  [Download PDF](#) [View Record in Scopus](#) [Google Scholar](#)

- [27] Y. Cao, A. Faghri
A numerical analysis of phase-change problem including natural convection
ASME J Heat Transf, 112 (1990), pp. 812-816
[CrossRef](#) [View Record in Scopus](#) [Google Scholar](#)
- [28] A. Faghri, Y. Zhang
Transport phenomena in multiphase systems
Elsevier Publications (2006)
[Google Scholar](#)
- [29] Y. Zhang, A. Faghri
Heat transfer enhancement in latent heat thermal energy storage system by using the internally finned tube
Int J Heat Mass Transf, 39 (15) (1996), pp. 3165-3173
[Article](#)  [Download PDF](#) [View Record in Scopus](#) [Google Scholar](#)
- [30] Y. Cao, A. Faghri
Performance characteristics of a thermal energy storage module: a transient pcm/forced convection conjugate analysis
Int J Heat Mass Transf, 34 (1991), pp. 93-101
[Article](#)  [Download PDF](#) [View Record in Scopus](#) [Google Scholar](#)
- [31] Y. Cao, A. Faghri
A study of thermal energy storage system with conjugate turbulent forced convection
ASME J Heat Transf, 114 (1992), pp. 1019-1027
[CrossRef](#) [View Record in Scopus](#) [Google Scholar](#)
- [32] R. Reid, B.E. Poling, J.M. Prausnitz
The properties of gases and liquids
(4th ed.), McGraw-Hill (1987)
[Google Scholar](#)
- [33] S.W. Churchill
Free convection around immersed bodies
E.U. Schlünder (Ed.), Heat exchanger design handbook, Hemisphere, New York (1983)
Section 2.5.7
[Google Scholar](#)
- [34] H.K. Versteeg, W. Malalasekera
An introduction to computational fluid dynamics: the finite volume method
Prentice Hall, London (1995)
[Google Scholar](#)
- [35] S.V. Patankar
Numerical heat transfer and fluid flow
McGraw-Hill, New York (1980)
[Google Scholar](#)
- [36] A. Bejan
Entropy generation minimization
CRC Press, New York (1996)
[Google Scholar](#)



Mustafa Asker has been working as an Assistant Professor in the Department of Mechanical Engineering at Engineering Faculty of Adnan Menderes University since 2014. He received B.Sc. and M.Sc. degrees in Mechanical Engineering from Al Nahrain Üniversitesi and his Ph.D. degree from Ege University.

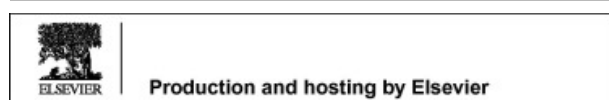


Hadi Ganjehsarabi is currently an assistant Professor in Mechanical Engineering at Erzincan University. He received his BS in Mechanical Engineering from Bou Ali Sina University in 2003, and his MS and PhD in Mechanical Engineering from Ege University in 2009 and 2014, respectively. He has also been a reviewer for several journals.



Mustafa Turhan Coban received his B.Sc. degree from Ege University Department of Mechanical Engineering in 1978, and his M.Sc. degree in Mechanical Engineering from Michigan Technological University (U.S.A.) in 1982. He graduated from University of Utah (U.S.A.) in 1986 with a Ph.D. in Mechanical Engineering. He is now assistant professor in Ege University. His research interests are fuel cell technologies, air conditioning and computer science.

Peer review under responsibility of Ain Shams University.



[Download](#) : [Download high-res image \(51KB\)](#)

[Download](#) : [Download full-size image](#)

© 2016 Ain Shams University. Production and hosting by Elsevier B.V.

ELSEVIER

[About ScienceDirect](#) [Remote access](#) [Shopping cart](#) [Advertise](#) [Contact and support](#) [Terms and conditions](#) [Privacy policy](#)

RELX™

We use cookies to help provide and enhance our service and tailor content and ads. By continuing you agree to the [use of cookies](#).

Copyright © 2020 Elsevier B.V. or its licensors or contributors. ScienceDirect® is a registered trademark of Elsevier B.V.

ScienceDirect® is a registered trademark of Elsevier B.V.